Electromagnetic form factors in the $N_f = 4$ holographic QCD

Hiwa A. Ahmed[1,2,*], Yidian Chen[3,†] and Mei Huang[1,‡]

[1]*School of Nuclear Science and Technology, University of Chinese Academy of Sciences, Beijing 100049, People's Republic of China*

[2]*Department of Physics, College of Science, Charmo University, 46023 Chamchamal, Sulaymaniyah, Iraq*

[3]*School of Physics, Hangzhou Normal University, Hangzhou 311121, People's Republic of China*

In this study, we employ a modified soft-wall holographic model with four flavors to investigate the meson spectra, decay constants, electromagnetic form factors, and charge radius of various mesons. We obtain the spectra for vector, axial vector, and pseudoscalar mesons. Decay constants are calculated and compared with experimental and lattice QCD data. The pion and kaon electromagnetic form factors are compared with the experimental data, and a good agreement is achieved for the kaon at low Q^2. For the charmed mesons, the electromagnetic form factors of the D and D_s and electric form factors of the D^* and D_s^* are well consistent with the lattice QCD data. Moreover, the electric, magnetic, and quadrupole form factors are predicted for the ρ, K^*, a_1, K_1, D_1, and D_{s1} mesons. Furthermore, the charge radius of the vector, axial vector, and pseudoscalars, including the strange and charmed mesons, are computed.

I. INTRODUCTION

Understanding the internal structure of hadrons involves studying electromagnetic form factors, which provide information about their magnetic moments and charge distributions. Since the electromagnetic form factors are nonperturbative quantities, one cannot use the quantum chromodynamics (QCD) to compute them. Experimental efforts have been underway for several decades to measure the electromagnetic form factors of light pseudoscalar mesons such as the pion and kaon. The pion and kaon form factors and their charge radius have been measured in Refs. [1–3], respectively. However, the experimental data for heavy mesons are not yet available. From a theoretical perspective, various nonperturbative approaches have been proposed in the literature; e.g., see details in Refs. [4–15]. Moreover, the lattice QCD approach has extensively studied the electromagnetic form factors and charge radii of both light and heavy mesons [16–21].

The holographic QCD approach as a low energy QCD model was established in the works of Refs. [22–36] for the light mesons with the features of the dynamical chiral

symmetry breaking. Extensions of this model have been made to include three flavors and flavor symmetry breaking due to the strange quark mass [37,38]. Recent developments have further extended the holographic QCD model to four flavors [39–41]. In Refs. [39,40], the masses of the ρ, ω, and J/ψ mesons are the same due to the fact that the mass term is zero in the 5D action. However, the masses of the axial vector and pseudoscalar mesons differ due to nonzero mass terms. In Ref. [41], an auxiliary scalar field was introduced to the action to explicitly break the $SU(4)_V$ symmetry to $SU(3)_V$, resulting in different mass values for the J/ψ meson.

The electromagnetic form factors have been investigated in the bottom-up holographic QCD model since the establishment of the model. For the first time, the pion electromagnetic form factor was studied in the hard-wall model in Ref. [42]. Similarly, in the work of [43], the pion electromagnetic form factor was discussed in the soft-wall model, and then they improved their previous results in Ref. [44] by considering a background field that interpolates between the hard-wall and soft-wall models. Furthermore, the kaon form factor was calculated within the hard wall-model [45,46], yielding results that align with experimental data within the uncertainties at the low Q^2. The pioneering work on the vector sector has been investigated in Refs. [47,48], where the ρ meson form factor and charge radius have been studied in the hard- and soft-wall models, respectively. By taking into account the flavor symmetry breaking, the electromagnetic form factor of the π, ρ, K, K^*, D, and D^* mesons investigated in the work of Ref. [39].

[*]hiwa.a.ahmed@mails.ucas.ac.cn

[†]chenyidian@hznu.edu.cn

[‡]huangmei@ucas.ac.cn

In the present paper, we follow the work of Ref. [41] and take the bottom-up holographic approach. Moreover, we include the higher-order potential in the 5D action. Below, we proceed by calculating the masses and decay constants of the π, K, η, D, D_s, ρ, K^*, ω, D^*, D_s^*, a_1, K_1, f_1, D_1, and D_{s1} mesons in the ground and excited states. Additionally, we predicted and compared the electromagnetic form factor of the pion and kaon mesons with the experimental data, and D and D_s mesons with the lattice QCD data. Moreover, for the vector mesons the electric, magnetic, and quadrupole form factors and charge radii of the ρ and K^* mesons are predicted; then when we compare the lattice results of D^* and D_S^* mesons, we obtain a good agreement. Finally, we predict the form factors and the charge radii of the axial vector mesons, a_1, K_1, D_1, and D_{s1}.

The paper is organized as follows. In Sec. II, we revisit the formalism of the bottom-up holographic QCD model for $N_f = 4$ flavor. Section III describes the equations of motion for vector, axial vector, and pseudoscalar fields derived from the second-order 5D action. Section IV presents the derivation of coupling constants, electromagnetic form factors, and charge radii from the three-point functions obtained from the cubic-order 5D action. The numerical results are presented in Sec. V. Finally, we conclude our work in Sec. VI.

II. THE HOLOGRAPHIC QCD MODEL FOR $N_f = 4$

In this section, we revisit the formalism of the bottom-up holographic QCD model, specifically focusing on the inclusion of the charm quark. The original formalism for the light flavor sector ($N_f = 2$) can be found in Refs. [22,24] for the hard-wall and soft-wall approaches, respectively. Additional works [37,39–41] discuss the extension of the model to include strange and charm quarks. Here, we mainly follow the conventions used in Ref. [41]. The five-dimensional metric defined in the anti–de Sitter (AdS) space is given by

$$ds^2 = \frac{1}{z^2}\left(\eta_{\mu\nu}dx^\mu dx^\nu + dz^2\right), \qquad (1)$$

where $\eta_{\mu\nu}$ is the four-dimensional metric in the Minkowski space, and z is the fifth dimension of the AdS space, which has an inverse energy scale. It is well known that in the AdS/CFT model for each operator in the 4D theory (also called boundary theory), there is a corresponding field in the 5D theory (bulk theory). The operators that are important for the chiral dynamics are left- and right-handed currents $J^a_{R/L\mu} = \bar{\psi}_{qR/L}\gamma_\mu t^a\psi_{qR/L}$ and quark bilinear $\bar{\psi}_{qL}\psi_{qR}$ which correspond to the R^a_μ and L^a_μ gauge fields and complex scalar fields X, respectively. Moreover, in Ref. [41] a heavy scalar field H and vector field V_H were introduced to describe the difference between the

mass of the light vector meson (ρ) and heavy charmed meson (J/ψ). Now, we have all the ingredients to write down the general five-dimensional action with $SU(4)_L \times SU(4)_R$ symmetry as follows.

$$
\begin{aligned}
S_M = -\int_\epsilon^{z_m} d^5x\sqrt{-g}e^{-\phi}\mathrm{Tr}\Big\{&(D^M X)^\dagger(D_M X) + M_5^2|X|^2 \\
&+ \frac{1}{4g_5^2}\left(L^{MN}L_{MN} + R^{MN}R_{MN}\right) \\
&+ (D^M H)^\dagger(D_M H) + M_5^2|H|^2\Big\},
\end{aligned}
\qquad (2)
$$

where $D^M X = \partial_M X - iL_M X + iX R_M$ and $D^M H = \partial_M H - iV_{HM} + iHV_{HM}$ are the covariant derivative of the scalar fields X and H, respectively, and $M_5^2 = (\Delta - p)(\Delta + p - 4) = -3$ where $\Delta = 3$ and $p = 0$. Despite introducing the dilaton field ϕ, a hard cutoff z_m is inserted as the upper limit of the model. So now the limits of the integration represent the IR (z_m) and UV (ϵ) regions. The coupling constant g_5 is related to the number of color (N_c) using the AdS/CFT dictionary $g_5^2 = 12\pi^2/N_c$ [22], where $N_c = 3$. The gauge field strengths L_{MN} and R_{MN} are defined by

$$
\begin{aligned}
L_{MN} &= \partial_M L_N - \partial_N L_M - i[L_M, L_N], \\
R_{MN} &= \partial_M R_N - \partial_N R_M - i[R_M, R_N].
\end{aligned}
\qquad (3)
$$

To simplify the analysis, the left- and right-handed gauge fields are replaced with the vector $[V_M = \frac{1}{2}(L_M + R_M)]$ and axial fields $[A_M = \frac{1}{2}(L_M - R_M)]$. The decomposition allows us to express the chiral gauge fields and the covariant derivative of the complex scalar field in terms of the vector and axial fields,

$$
\begin{aligned}
V_{MN} &= \partial_M V_N - \partial_N V_M - i[V_M, V_N] - i[A_M, A_N], \\
A_{MN} &= \partial_M A_N - \partial_N A_M - i[V_M, A_N] - i[A_M, V_N], \\
D^M X &= \partial_M X - i[V_M, X] - i\{A_M, X\}.
\end{aligned}
\qquad (4)
$$

The complex scalar field can be decomposed as

$$X = e^{i\pi}X_0 e^{i\pi}, \qquad (5)$$

where $X_0 = \frac{1}{2}\mathrm{diag}[v_u(z), v_d(z), v_s(z), v_c(z)]$ the vacuum expectation value, and π is the pseudoscalar field. Moreover, The action also includes a dilaton field ϕ. In the original hard-wall model [22], it is impossible to get the mesons' linear mass trajectories. To overcome the issue, a quadratic dilaton field is introduced in Ref. [24] that only depends on the fifth dimension z,

$$\phi(z \to \infty) = \mu^2 z^2, \qquad (6)$$

where μ is related to the Regge slope and sets the mass scale for the meson spectrum.

To study the behavior of the background X_0 and find the vacuum expectation value, one needs to turn off all the fields in the action [Eq. (2)] except the background. The equation of motion for the scalar vacuum expectation value $v_{q=l,s,c}(z)$ with $l = u$, d is obtained as

$$-\frac{z^3}{e^{-\phi}} \partial_z \frac{e^{-\phi}}{z^3} \partial_z v_q(z) - \frac{3}{z^2} v_q(z) = 0. \qquad (7)$$

The analytical solutions of Eq. (7) are given by the Tricomi confluent hypergeometric function $U(a, b, y)$ and the generalized Laguerre polynomial L.

$$v_q(z) = C_{q1} z \sqrt{\pi} U\left(\frac{1}{2}, 0, \phi\right) - C_{q2} z L\left(-\frac{1}{2}, -1, \phi\right) \qquad (8)$$

As reported in [49], the second part of the solution must be disregarded to get a finite action at the IR region. In the UV region, Eq. (8) expands to

$$v_q(z)|_{z \to 0} = 2C_{q1} z + C_{q1}\left[-\mu^2 + 2\gamma_E \mu^2 + 2\mu^2 \log z \right.$$
$$\left. + 2\mu^2 \log \mu + \mu^2 \Psi\left(\frac{3}{2}\right)\right] z^3. \qquad (9)$$

Comparing this solution to the UV behavior of the chiral condensate in the hard-wall model $[v_q(z) = m_q z + \sigma_q z^3]$ [22], one can notice that the quark mass is $m_q = 2C_{q1}$ and the quark condensate σ_q is also proportional with C_{q1}. Now, spontaneous and explicit chiral symmetry breaking is related. In contradiction with QCD, in the massless limit, the spontaneous chiral symmetry vanishes [50]. As pointed out in Ref. [24], the issue is present because the equation of motion is linear in $v_q(z)$. A modified dilaton profile was proposed in [51], and this work also considers higher-order potential to solve this issue by adding higher-order terms in the scalar potential that can remedy it [24].

In Ref. [50], a higher-order term (quartic term) in the potential $V(X)$ is added to the $5D$ action,

$$S_M = -\int_\epsilon^{z_m} d^5 x \sqrt{-g} e^{-\phi} \text{Tr}\left\{ (D^M X)^\dagger (D_M X) + M_5^2 |X|^2 \right.$$
$$- \kappa |X|^4 + \frac{1}{2g_5^2} \left(V^{MN} V_{MN} + A^{MN} A_{MN}\right)$$
$$\left. + (D^M H)^\dagger (D_M H) + M_5^2 |H|^2 \right\}, \qquad (10)$$

where κ is a parameter and can be determined. Keeping only the background in the action, the zeroth order of the action is given by

$$S^{(0)} = -\frac{1}{4} \int_\epsilon^{z_m} d^5 x \left\{ \frac{e^{-\phi(z)}}{z^3} \left(2v_l'(z) v_l'(z) + v_s'(z) v_s'(z) + v_c'(z) v_c'(z)\right) - \frac{e^{-\phi(z)}}{z^5} \left(3\left(2v_l(z)^2 + v_s(z)^2 + v_c(z)^2\right)\right. \right.$$
$$\left. \left. - \frac{\kappa}{4}\left(2v_l(z)^4 + v_s(z)^4 + v_c(z)^4\right)\right) + \frac{e^{-\phi(z)}}{z^3}\left(h_c'(z) h_c'(z)\right) - \frac{3e^{-\phi(z)}}{z^5} h_c(z)^2 \right\}. \qquad (11)$$

Now, the equation of motion for the scalar vacuum expectation value is not linear anymore and becomes

$$-\frac{z^3}{e^{-\phi}} \partial_z \frac{e^{-\phi}}{z^3} \partial_z v_q(z) - \frac{3}{z^2} v_q(z) - \frac{\kappa}{2z^2} v_q^3(z) = 0. \qquad (12)$$

An appropriate parametrization that respects the UV and IR asymptotic behavior of the vacuum expectation value is given in Ref. [50]

$$v(z) = az + bz \tanh(cz^2), \qquad (13)$$

with the definitions for parameters a, b, and c as

$$a = \frac{\sqrt{3} m_q}{g_5}, \qquad b = \sqrt{\frac{4\mu^2}{\kappa}} - a, \qquad c = \frac{g_5 \sigma}{\sqrt{3} b}. \qquad (14)$$

Now $v(z)$ in Eq. (13) satisfies the UV and IR behavior at small and large z,

$$v(z \to 0) = az + bcz^3 + \mathcal{O}(z^5), \qquad (15)$$

$$v(z \to \infty) = (a + b)z = \sqrt{\frac{4\mu^2}{\kappa}} z. \qquad (16)$$

Furthermore, one can obtain the dilaton profile by substituting Eq. (13) into (12) and solving the following equation for $\phi(z)$:

$$\phi'(z) = \frac{1}{\partial_z v_q(z)} \left[z^3 \partial_z \frac{1}{z^3} \partial_z v_q(z) + \frac{3}{z^2} v_q(z) + \frac{\kappa}{2z^2} v_q^3(z) \right], \qquad (17)$$

where the asymptotic behavior of the dilaton profile is obtained as the following:

$$\phi(z \to 0) = \frac{\kappa}{4} a^2 z^2 + \mathcal{O}(z^6), \qquad (18)$$

$$\phi(z \to \infty) = \frac{\kappa}{4}(a+b)^2 z^2 = \mu^2 z^2. \qquad (19)$$

It is worth pointing out that the dilaton profile in Eq. (17) depends on the quark flavor, and for each flavor one can obtain a different dilaton profile. This behavior can be clearly seen in the UV asymptotic behavior of $\phi(z \to 0)$ in Eq. (18), where ϕ is proportional to the square of the quark mass. Conversely, the IR behavior of the ϕ field is similar to the one used in the original soft-wall model [24] and does not depend on the quark mass. This IR behavior secures the linear trajectories of the mass spectra. In order to avoid the flavor dependence of the dilaton profile and guarantee the linear Regge slope, we use the IR asymptotic behavior of the ϕ field in the present work. It is also noticed that comparing with the modified dilaton profile proposed in [51], where there is a negative quadratic dilaton at UV and a positive quadratic dilaton at IR, our solution obtained in Eqs. (18) and (19) requires positive quadratic dilaton at both UV and IR.

Similar to the bilinear field X, the auxiliary field H is a diagonal matrix. However, it only reflects the effect of the charm quark mass, $H = \frac{1}{2}\text{diag}[0, 0, 0, h_c(z)]$. Then, h_c at the UV boundary should behave like $h_c(z \to \infty) = m_{hc}z$. To get such a behavior, we assume that $h_c = az$, where the value of m_{hc} is different from the charm quark mass used in Eq. (13).

III. EQUATIONS OF MOTION

In the AdS/CFT model, one can find the mass eigenvalues by solving the equation of motion of each particular field. The equation of motion can be found from the expansion of the action in Eq. (10) up to the second order in the fields V_M, A_m, and π. The fields V_M, A_m, and π in Eq. (10) expanded to $V_M^a t^a$, $A_m^a t^a$, and $\pi^a t^a$, respectively, where t^a, $a = 1, 2, \dots, 15$ are the generators of $SU(4)$ group which satisfy $\text{Tr}(t^a t^b) = \frac{1}{2}\delta^{ab}$. Now we can write the action up to the second order as the following:

$$S^{(2)} = -\int d^5x \left\{ \eta^{MN} \frac{e^{-\phi(z)}}{z^3} \left((\partial_M \pi^a - A_M^a)(\partial_N \pi^b - A_N^b) M_A^{ab} - V_M^a V_N^b M_V^{ab} + V_{HM}^a V_{HN}^b M_{V_H}^{ab} \right) \right.$$
$$\left. + \frac{e^{-\phi(z)}}{4g_5^2 z} \eta^{MP} \eta^{NQ} (V_{MN}^a V_{PQ}^b + A_{MN}^a A_{PQ}^b) \right\}, \qquad (20)$$

where η^{MN} is the metric in 5D Minkowski space which is $\eta^{MN} = \text{diag}[-1, 1, 1, 1, 1]$, $V_{MN}^a = \partial_M V_N^a - \partial_N V_M^a$, and $A_{MN}^a = \partial_M A_N^a - \partial_N A_M^a$. The vector, axial, and pseudoscalar fields are described by 4×4 matrices,

$$V = V^a t^a = \frac{1}{\sqrt{2}} \begin{pmatrix} \frac{\rho^0}{\sqrt{2}} + \frac{\omega'}{\sqrt{6}} + \frac{\psi}{\sqrt{12}} & \rho^+ & K^{*+} & \bar{D}^{*0} \\ \rho^- & -\frac{\rho^0}{\sqrt{2}} + \frac{\omega'}{\sqrt{6}} + \frac{\psi}{\sqrt{12}} & K^{*0} & D^{*-} \\ K^{*-} & \bar{K}^{*0} & -\sqrt{\frac{2}{3}}\omega' + \frac{\psi}{\sqrt{12}} & D_s^{*-} \\ D^{*0} & D^{*+} & D_s^{*+} & -\frac{3}{\sqrt{12}}\psi \end{pmatrix}, \qquad (21)$$

$$A = A^a t^a = \frac{1}{\sqrt{2}} \begin{pmatrix} \frac{a_1^0}{\sqrt{2}} + \frac{f_1}{\sqrt{6}} + \frac{\chi_{c1}}{\sqrt{12}} & a_1^+ & K_1^+ & \bar{D}_1^0 \\ a_1^- & -\frac{a_1^0}{\sqrt{2}} + \frac{f_1}{\sqrt{6}} + \frac{\chi_{c1}}{\sqrt{12}} & K_1^0 & D_1^- \\ K_1^- & \bar{K}_1^0 & -\sqrt{\frac{2}{3}}f_1 + \frac{\chi_{c1}}{\sqrt{12}} & D_{s1}^- \\ D_1^0 & D_1^+ & D_{s1}^+ & -\frac{3}{\sqrt{12}}\chi_{c1} \end{pmatrix}, \qquad (22)$$

$$\pi = \pi^a t^a = \frac{1}{\sqrt{2}} \begin{pmatrix} \frac{\pi^0}{\sqrt{2}} + \frac{\eta}{\sqrt{6}} + \frac{\eta_c}{\sqrt{12}} & \pi^+ & K^+ & \bar{D}^0 \\ \pi^- & -\frac{\pi^0}{\sqrt{2}} + \frac{\eta}{\sqrt{6}} + \frac{\eta_c}{\sqrt{12}} & K^0 & D^- \\ K^- & \bar{K}^0 & -\sqrt{\frac{2}{3}}\eta + \frac{\eta_c}{\sqrt{12}} & D_s^- \\ D^0 & D^+ & D_s^+ & -\frac{3}{\sqrt{12}}\eta_c \end{pmatrix}. \qquad (23)$$

The mass terms in the action M_A^{ab}, M_V^{ab}, and $M_{V_H}^{ab}$ are defined by

$$M_A^{ab}\delta^{ab} = \text{Tr}(\{t^a, X_0\}\{t^b, X_0\}),$$
$$M_V^{ab}\delta^{ab} = \text{Tr}([t^a, X_0][t^b, X_0]),$$
$$M_{V_H}^{ab} = \text{Tr}([H, t^a][H, t^b]), \tag{24}$$

where $M_{V_H}^{a,b}$ is zero except for the case $a = b = 15$. The vector field in Eq. (20) satisfies the following equation of motion:

$$-\partial^M \frac{e^{-\phi}}{g_5^2 z} V_{MN}^a - \frac{e^{-\phi}}{z^3}\left(M_V^{aa} V_M^a - M_{V_H}^{aa} V_{HM}^a\right) = 0, \tag{25}$$

where $V_M^a = (V_\mu^a, V_z^a)$. The gauge fixing for the vector field is $V_z^a = 0$ and for the transverse part of the vector field ($V_\mu^a = V_{\mu\perp}^a + V_{\mu\|}^a$), $\partial^\mu V_{\mu\perp}^a = 0$. Applying the decomposition and gauge choices, Eq. (25) reduces to the following form:

$$\left(-\frac{z}{e^{-\phi}}\partial_z \frac{e^{-\phi}}{z}\partial_z + \frac{2g_5^2(M_{V_H}^{aa} - M_V^{aa})}{z^2}\right)V_{\mu\perp}^a(q, z)$$
$$= -q^2 V_{\mu\perp}^a(q, z), \tag{26}$$

where $V_{\mu\perp}^a(q, z)$ is the 4D Fourier transform of $V_{\mu\perp}^a(x, z)$. According to the AdS/CFT conjecture, one can write the vector field according to the bulk-to-boundary propagator and its boundary value at UV, which acts as a Fourier transform of the source of the 4D conserved vector current operator, $V_{\mu\perp}^a(q, z) = V_{\mu\perp}^{0a}(q)\mathcal{V}^a(q^2, z)$. It is worth knowing that the bulk-to-boundary propagator $\mathcal{V}^{0a}(q^2, z)$ satisfies the equation of motion for the vector field with the boundary condition $\mathcal{V}^a(q^2, \epsilon) = 1$ and $\partial_z \mathcal{V}^a(q^2, zm) = 0$. To find the mass eigenvalues of the vector mesons, we need a wave function $\psi_V(z)$ with $-q^2 = m_V^2$, which satisfies Eq. (26) with the boundary conditions $\psi_{V^n}(\epsilon) = 0$ and $\partial_z\psi_{V^n}(zm) = 0$, and normalized as $\int dz \frac{e^{-\phi}}{z}\psi_V^n(z)\psi_V^m(z) = \delta^{nm}$. Moreover, the bulk-to-boundary propagator can be written as a sum over meson poles.

$$\mathcal{V}^a(q^2, z) = \sum_n \frac{-g_5 f_{V^n}^a \psi_{V^n}^a(z)}{q^2 - m_{V^n}^a{}^2}, \tag{27}$$

where $f_{V^n}^a = |\partial_z\psi_{V^n}^a(\epsilon)/(g_5\epsilon)|$ is the decay constant of the nth mode of the vector meson [22].

The equation of motion for the axial vector field is similar to the vector field, except the auxiliary field H does not contribute. The axial vector field A_μ^a can be decomposed to the transverse and longitudinal parts, $A_\mu^a = A_{\mu\perp}^a + A_{\mu\|}^a$,

where $A_{\mu\|}^a = \partial_\mu\phi^a$ has the contribution to the pseudoscalar mesons. The equation of motion derived from Eq. (10) is given by

$$\left(-\frac{z}{e^{-\phi}}\partial_z \frac{e^{-\phi}}{z}\partial_z + \frac{2g_5^2 M_A^{aa}}{z^2}\right)A_{\mu\perp}^a(q, z) = -q^2 A_{\mu\perp}^a(q, z), \tag{28}$$

with the gauge fixing and transverse condition $A_z^a = 0$, and $\partial^\mu A_{\mu\perp}^a$, respectively. The bulk-to-boundary propagator of the axial vector field $\mathcal{A}^a(q^2, z)$ satisfies the boundary conditions, $\mathcal{A}^a(q^2, \epsilon) = 0$ and $\partial_z\mathcal{A}^a(q^2, zm) = 0$, in the UV and IR region.

Finally, the mass spectra of the pseudoscalar mesons can be found by solving the coupled equation of motions between the pseudoscalar field π and the longitudinal part of the axial vector field ϕ,

$$q^2\partial_z\varphi^a(q, z) + \frac{2g_5^2 M_A^{aa}}{z^2}\partial_z\pi^a(q, z) = 0,$$
$$\frac{z}{e^{-\phi}}\partial_z\left(\frac{e^{-\phi}}{z}\partial_z\varphi^a(q, z)\right) - \frac{2g_5^2 M_A^{aa}}{z^2}\left(\varphi^a(q, z) - \pi^a(q, z)\right) = 0, \tag{29}$$

with the boundary conditions $\pi^a(q^2, \epsilon) = \phi^a(q^2, \epsilon) = 0$ and $\partial_z\pi^a(q^2, zm) = \partial_z\phi^a(q^2, zm) = 0$. In the holographic QCD approach, the decay constants for the vector, axial vector, and pseudoscalar mesons are defined by

$$f_{V^n}^a = \frac{e^{-\phi}}{g_5 z}\partial_z\psi_{V^n}^a(z)\Big|_{z\to\epsilon},$$
$$f_{A^n}^a = \frac{e^{-\phi}}{g_5 z}\partial_z\psi_{A^n}^a(z)\Big|_{z\to\epsilon},$$
$$f_{\pi^n}^a = -\frac{e^{-\phi}}{g_5 z}\partial_z\varphi^{a,n}(z)\Big|_{z\to\epsilon}, \tag{30}$$

where $\psi_{V^n}^a(z)$, $\psi_{A^n}^a(z)$, and $\varphi^{a,n}(z)$ are the normalized wave functions for the vector, axial vector, and pseudoscalar mesons, respectively.

IV. THREE-POINT INTERACTION COUPLING CONSTANTS AND FORM FACTORS

The coupling constants and form factors can be obtained from the cubic order of the 5D action in Eq. (10),

$$S^{(3)} = -\int d^5x \Big\{ \eta^{MN} \frac{e^{-\phi(z)}}{z^3} \big(2(A_M^a - \partial_M \pi^a) V_N^b \pi^c g^{abc}$$
$$+ V_M^a \big(\partial_N(\pi^b \pi^c) - 2A_M^b \pi^c\big) h^{abc} - V_M^a V_N^b \pi^c k^{abc}\big)$$
$$+ \frac{e^{-\phi(z)}}{2g_5^2 z} \eta^{MP} \eta^{NQ} \big(V_{MN}^a V_P^b V_Q^c + V_{MN}^a A_P^b A_Q^c$$
$$+ A_{MN}^a V_P^b A_Q^c + A_{MN}^a A_P^b V_Q^c\big) f^{bca} \Big\} \tag{31}$$

with the following definitions for g^{abc}, h^{abc}, and k^{abc}:

$$g^{abc} = iTr(\{t^a, X_0\}[t^b, \{t^c, X_0\}]),$$
$$h^{abc} = iTr([t^a, X_0]\{t^b, \{t^c, X_0\}\}),$$
$$k^{abc} = -2Tr([t^a, X_0][t^b, \{t^c, X_0\}]). \tag{32}$$

In the present work, we are interested in the three-point interactions of the VVV, VAA, and $V\pi\pi$. The corresponding part of the action to these three-point interactions are

$$S_{VVV} = -\int_\epsilon^{z_m} d^5 \frac{e^{-\phi(z)}}{2g_5^2 z} \eta^{mp} \eta^{nq} \big(V_{mn}^a V_p^b V_q^c\big) f^{abc} \tag{33}$$

$$S_{VAA} = -\int_\epsilon^{z_m} d^5 \frac{e^{-\phi(z)}}{2g_5^2 z} \eta^{mp} \eta^{nq} \big(V_{mn}^a A_p^b A_q^c + A_{mn}^a V_p^b A_q^c + A_{mn}^a A_p^b V_q^c\big) f^{abc} \tag{34}$$

$$S_{V\pi\pi} = -\int_\epsilon^{z_m} d^5x \Big\{ \eta^{mn} \frac{e^{-\phi(z)}}{z^3} \big(2(A_m^a - \partial_m \pi^a) V_n^b \pi^c g^{abc}$$
$$+ V_m^a(\partial_n(\pi^b \pi^c) - 2A_n^b \pi^c) h^{abc})$$
$$+ \frac{e^{-\phi(z)}}{2g_5^2 z} \eta^{mp} \eta^{nq} (V_{mn}^a A_p^b A_q^c) f^{abc} \Big\}. \tag{35}$$

In the AdS/CFT approach, the coupling constants of three-point interaction can be obtained from the three-point correlation functions by functional variation of the 5D action with respect to the sources of the 5D fields [42,44]. The relevant coupling constants calculated are given by

$$g_{VVV} = g_5 f^{abc} \int_\epsilon^{zm} dz \frac{e^{-\phi(z)}}{z} V^a(z) V^b(z) V^c(z), \tag{36}$$

$$g_{VAA} = g_5 f^{abc} \int_\epsilon^{zm} dz \frac{e^{-\phi(z)}}{z} V^a(z) A^b(z) A^c(z), \tag{37}$$

$$g_{V\pi\pi} = g_5 \int_\epsilon^{zm} dz \frac{e^{-\phi(z)}}{z} \Big(f^{abc} \partial_z \phi^a V^b(z) \partial_z \phi^a$$
$$- \frac{2g_5^2}{z^2} (\pi^a - \phi^a) V^b(z) (\pi^c - \phi^c) \big(g^{abc} - h^{bac}\big) \Big). \tag{38}$$

Moreover, we study the electromagnetic (EM) form factors of the channels VVV, VAA, and $V\pi\pi$ and the charge radius. The EM form factors of the vector, axial vector, and pseudoscalar mesons are defined by [39,42,52]

$$\langle V^a(p+q), \epsilon'|J_{EM}^\mu(0)|V^a(p), \epsilon \rangle$$
$$= -(\epsilon' \cdot \epsilon)(2p+q)^\mu F_{V^a}^1(q^2) + [\epsilon'^\mu(\epsilon \cdot q) - \epsilon^\mu(\epsilon' \cdot q)]$$
$$\times [F_{V^a}^1(q^2) + F_{V^a}^2(q^2)] + \frac{1}{M_{V^a}^2} (q \cdot \epsilon')(q \cdot \epsilon)$$
$$\times (2p+q)^\mu F_{V^a}^3(q^2), \tag{39}$$

$$\langle A^a(p+q), \epsilon'|J_{EM}^\mu(0)|A^a(p), \epsilon \rangle$$
$$= -(\epsilon' \cdot \epsilon)(2p+q)^\mu F_{A^a}^1(q^2) + [\epsilon'^\mu(\epsilon \cdot q) - \epsilon^\mu(\epsilon' \cdot q)]$$
$$\times [F_{A^a}^1(q^2) + F_{A^a}^2(q^2)] + \frac{1}{M_{A^a}^2} (q \cdot \epsilon')(q \cdot \epsilon)$$
$$\times (2p+q)^\mu F_{A^a}^3(q^2), \tag{40}$$

$$\langle \pi^a(p+q)|J_{EM}^\mu(0)|\pi^a(p) \rangle = (2p+q)^\mu F_{\pi^a}(q^2), \tag{41}$$

where ϵ and ϵ' are the polarization vectors of the initial and final vector mesons, respectively, and $J_{EM}^\mu(0)$ is the electromagnetic current. The electromagnetic current can be represented by the linear combination of the flavor currents via [39]

$$J_{EM}^\mu(x) = \sum_{a=(\rho,\omega,J/\psi)} c_a J_a^\mu(x), \tag{42}$$

where the coefficient c_a is a constant depending on the contribution of the quarks in the EM current. The electric (charge), magnetic, and quadrupole form factors of the vector and axial vector mesons can be deduced from the linear combination of the form factors in Eqs. (39) and (40), respectively.

$$F_{V^a}^E = F_{V^a}^1 + \frac{q^2}{6M_{V^a}^2} \Big[F_{V^a}^2 - \Big(1 - \frac{q^2}{4M_{V^a}^2}\Big) F_{V^a}^3 \Big],$$

$$F_{V^a}^M = F_{V^a}^1 + F_{V^a}^2,$$

$$F_{V^a}^Q = -F_{V^a}^2 + \Big(1 - \frac{q^2}{4M_{V^a}^2}\Big) F_{V^a}^3. \tag{43}$$

$$F_{A^a}^E = F_{A^a}^1 + \frac{q^2}{6M_{A^a}^2}\left[F_{A^a}^2 - \left(1 - \frac{q^2}{4M_{A^a}^2}\right)F_{A^a}^3\right],$$

$$F_{A^a}^M = F_{A^a}^1 + F_{A^a}^2,$$

$$F_{A^a}^Q = -F_{A^a}^2 + \left(1 - \frac{q^2}{4M_{A^a}^2}\right)F_{A^a}^3. \tag{44}$$

For the elastic case, the electromagnetic form factors obtained as

$$F_{V^a}^1 = F_{V^a}^2 = F_{V^a} = \sum_n \frac{f_{V^a}g_{VVV}}{M_{V^a}^2 + Q^2},$$

$$F_{V^a}^3 = 0, \tag{45}$$

$$F_{A^a}^1 = F_{A^a}^2 = F_{A^a} = \sum_n \frac{f_{V^a}g_{VAA}}{M_{V^a}^2 + Q^2},$$

$$F_{A^a}^3 = 0, \tag{46}$$

$$F_{\pi^a} = \sum_n \frac{f_{V^a}g_{V\pi\pi}}{M_{V^a}^2 + Q^2}, \tag{47}$$

where $Q^2 = -q^2$. Using the couplings in Eqs. (36)–(38) and the definition of the bulk to boundary in Eq. (27), one can reach the final version of the form factors for the vector, axial vector, and pseudoscalar mesons,

$$F_V(Q^2) = f^{abc}\int dz\,\frac{e^{-\phi(z)}}{z}\mathcal{V}^a(Q^2,z)V^b(z)V^c(z), \tag{48}$$

$$F_A(Q^2) = f^{abc}\int dz\,\frac{e^{-\phi(z)}}{z}\mathcal{V}^a(Q^2,z)A^b(z)A^c(z), \tag{49}$$

$$F_\pi(Q^2) = \int dz\,\frac{e^{-\phi(z)}}{z}\mathcal{V}^b(Q^2,z)\left(f^{abc}\partial_z\phi^a\partial_z\phi^c\right.$$
$$\left. - \frac{2g_5^2}{z^2}(\pi^a - \phi^a)(\pi^c - \phi^c)(g^{abc} - h^{bac})\right). \tag{50}$$

Note that the bulk-to-boundary propagator for vector sector $\mathcal{V}^b(Q^2,z)$ can be obtained by solving the equation of motion, Eq. (26). The analytical solution of Eq. (26) can be obtained only for the off-shell mode of the ρ meson; for others, one has to use the numerical method. The solution reads

$$\mathcal{V}^b(Q^2,z) = \Gamma\left(1 + \frac{Q^2}{4\mu^2}\right)U\left(\frac{Q^2}{4\mu^2},0,z^2\mu^2\right). \tag{51}$$

The charge radius can be obtained from the low Q^2 expansion of the EM form factors of a pseudoscalar meson and the charge form factors of the vector meson,

$$F^{(C)}(Q^2) = 1 - \frac{1}{6}\langle r^2\rangle Q^2 + \cdots, \tag{52}$$

then, the charge radius is given by

$$\langle r^2\rangle = -6\frac{dF(Q^2)}{dQ^2}\bigg|_{Q^2\to0}. \tag{53}$$

V. RESULTS

This section presents the numerical results for the meson spectra, decay constants, electromagnetic form factor, and charge radii obtained from our holographic QCD model. The model incorporates various free parameters, such as μ, m_u, m_s, m_c, m_{hc}, σ_u, σ_s, σ_c, z_m, and κ. The values of these parameters are determined by fitting the model with the experimental value of the mass and decay constant of the following mesons, m_ρ, m_π, f_π, m_{a_1}, m_K, f_K, m_{η_c}, $m_{\chi_{c1}}$, $m_{J/\psi}$, and $m_{\psi(3770)}$. The values of the parameters obtained from the fitting are provided in Table I.

A. Meson spectra

Once the parameters are fixed, the model enables the calculation of meson spectra and decay constants for vector, axial vector, and pseudoscalar mesons. The masses of vector mesons are determined by solving the equation of motion given in Eq. (26), where $m_V^2 = -q^2$. Similarly, by solving Eqs. (28) and (29), one can get the masses of the axial vector and pseudoscalar mesons. The resulting meson masses compared to the values listed by the Particle Data Group (PDG) [53] are presented in Tables II–IV for vector, axial vector, and pseudoscalar mesons, respectively. Considering the exact $SU(4)_V$ symmetry, the masses of the ρ, ω, and J/ψ mesons should be equal. As a consequence of the $SU(4)_V$ symmetry, we can see that from Table II, the masses of the ground and excited states of the ρ and ω mesons are exactly the same. However, the mass of the J/ψ meson differs because of the explicit symmetry breaking of the action by introducing an auxiliary field H. For the case of D^* and D_s^* mesons, the inclusion of the nonzero value of M_V^{aa} in the equation of motion [Eq. (25)] leads an explicit $SU(4)$ flavor symmetry breaking. In addition, for the case of the axial vector and pseudoscalar mesons, the mass term M_A^{aa} is nonzero for all the mesons, and then the chiral symmetry is explicitly broken by the different values of the quark masses for all the axial vector and pseudoscalar mesons. Moreover,

TABLE I. The values of the free parameters with the unit of MeV.

$\mu = 430$	$\sigma_u = (296.2)^3$
$m_u = 3.2$	$\sigma_s = (259.8)^3$
$m_s = 142.3$	$\sigma_c = (302)^3$
$m_c = 1597.1$	$z_m = 10000$
$m_{hc} = 1985$	$\kappa = 30$

TABLE II. Comparison of the vector mesons masses with the values listed in PDG [53].

n	m_ρ	Experiment	m_{K^*}	Experiment	m_ω	Experiment	m_{D^*}	Experiment	$m_{D_s^*}$	Experiment	$m_{J/\psi}$	Experiment
1	860	775	860.05	892	860	782	1914.90	2007	1911.40	2112	3099.21	3097
2	1216.24	1465	1216.29	1414	1216.24	1410	2110.04	2627	2107.36	2714	3329.54	3686
3	1490.09	1570	1490.15	1718	1490.09	1670	2286.48	2781			3702.95	3733
4	1726.63	1720			1726.63	1960					3863.62	4040
5	1957.02	1900			1957.02	2205						
6	2201.44	2150			2201.44	2290						
7					2462.12	2330						

TABLE III. Comparison of the axial vector mesons masses with the values listed in PDG [53].

n	m_{a_1}	Experiment	m_{K_1}	Experiment	m_{f_1}	Experiment	m_{D_1}	Experiment	$m_{D_{s1}}$	Experiment	$m_{\chi_{c1}}$	Experiment
1	1286.95	1230	1287.67	1253	1287.97	1282	2641.47	2422	2657.55	2460	3511.04	3511
2	1541.88	1411	1542.90	1403	1543.32	1426					4050.30	3872
3	1765.28	1655	1766.30	1672	1766.73	1518					4149.46	4147
4	1968.94	1930			1970.32	1971					4340.88	4274
5	2172.45	2096			2173.82	2310						
6	2393.35	2270										

TABLE IV. Comparison of the pseudoscalar mesons masses with the values listed in PDG [53].

n	m_{π^0}	Experiment	m_{K^0}	Experiment	m_η	Experiment	m_{D^0}	Experiment	$m_{D_s^\pm}$	Experiment	m_{η_c}	Experiment
1	141.69	139.57	622.15	498	740.52	548	2032.67	1865	2114.32	1968	2968.46	2984
2	1439.04	1300	1451.28	1482	145.78	1294	2913.25	2549			3894.14	3637
3	1698.20	1810	1709.18	1629	1716.10	1475						
4	2124.64	2070	1927.17	1874	1933.92	1751						
5	2345.61	2360			2142.68	2010						

comparing our meson spectra with the one obtained in Ref. [41], one can conclude that our results are well improved, especially for the pseudoscalar mesons. This improvement comes from the inclusion of the higher-order terms in the scalar potential.

B. Decay constant

The calculated decay constants are presented in Table V for various mesons within our model. In the vector meson sector, we compared the decay constant of the ρ meson to the experimental value obtained from Ref. [54]. Our result shows a discrepancy of 16% compared to the experimental value. Additionally, we predicted the decay constants for the K^*, D^*, and D_s^* mesons. Moving to the axial vector sector, only the experimental value for the a_1 meson (taken from Ref. [55]) is available for the comparison, while the decay constants of the other axial vector mesons are predicted in our model. Notably, the predicted value for the a_1 meson aligns well with the experimental value. In the pseudoscalar sector, the decay constants of the pion and kaon are found to be compatible with the values listed in

TABLE V. The predicted decay constants calculated from the hQCD compared to experimental or lattice data.

Observable	$N_f = 4$, hQCD (MeV)	Measured (MeV)
$f_\rho^{1/2}$	288.50	345 [54]
$f_{K^*}^{1/2}$	288.28	
$f_{D^*}^{1/2}$	413.36	
$f_{D_s^*}^{1/2}$	427.78	
$f_{a_1}^{1/2}$	351.34	354 [55]
$f_{K_1}^{1/2}$	348.26	
$f_{f_1}^{1/2}$	346.79	
$f_{D_1}^{1/2}$	502.11	
$f_{D_{s1}}^{1/2}$	475.74	
f_π	91.03	92.07 [53]
f_K	108.5	110 [53]
f_η	126.32	
f_{D^0}	199.31	149.8 [53]
f_{D_s}	197.73	176.1 [53]

PDG [53]. However, for the D^0 and D_s mesons, there are only results from lattice QCD studies, and no experimental data is directly comparable in this context. Similar to the meson spectra, the decay constants of our work have better compatibility with the experimental and lattice data compare to Ref. [41].

C. Three-particle coupling constant

In our analysis of three-point functions, we have calculated the coupling constants for three types of interactions: VVV (vector-vector-vector), VAA (vector-axial vector-axial vector), and $V\pi\pi$ (vector-pseudoscalar-pseudoscalar). It is worth noting that, assuming the equal masses and condensates for the quarks, the couplings should satisfy the following relations, which is the manifestation of flavor symmetry restoration,

$$g_{\rho KK} = g_{\rho DD} = \frac{1}{2} g_{\rho\pi\pi},$$

$$g_{\rho K^* K^*} = g_{\rho D^* D^*} = \frac{1}{2} g_{\rho\rho\rho},$$

$$g_{\rho K_1 K_1} = g_{\rho D_1 D_1} = \frac{1}{2} g_{\rho a_1 . a_1}. \qquad (54)$$

TABLE VI. Reporting the flavor symmetry breaking in our calculations.

$SU(4)$ symmetry relation	Violation in $N_f = 4$, hQCD (%)
$2g_{\rho KK}/g_{\rho\pi\pi}$	14
$2g_{\rho DD}/g_{\rho\pi\pi}$	47
$2g_{\rho K^* K^*}/g_{\rho\rho\rho}$	0
$2g_{\rho D^* D^*}/g_{\rho\rho\rho}$	36
$2g_{\rho K_1 K_1}/g_{\rho a_1 a_1}$	1
$2g_{\rho D_1 D_1}/g_{\rho a_1 a_1}$	76

The numerical value of the ratios between the strong coupling constants are reported in Table VI. The $SU(4)$ flavor symmetry is clearly seen in Table VI, where the symmetry is badly broken in the case of including the charm quark. Similar results are reported in the hard-wall model [39] and QCD sum rules [56].

D. Form factor

We present the results of the meson form factors obtained using the definitions of EM form factors described in the previous section. First, we focus on the vector meson form factors and display them in Fig. 1. The form factors at
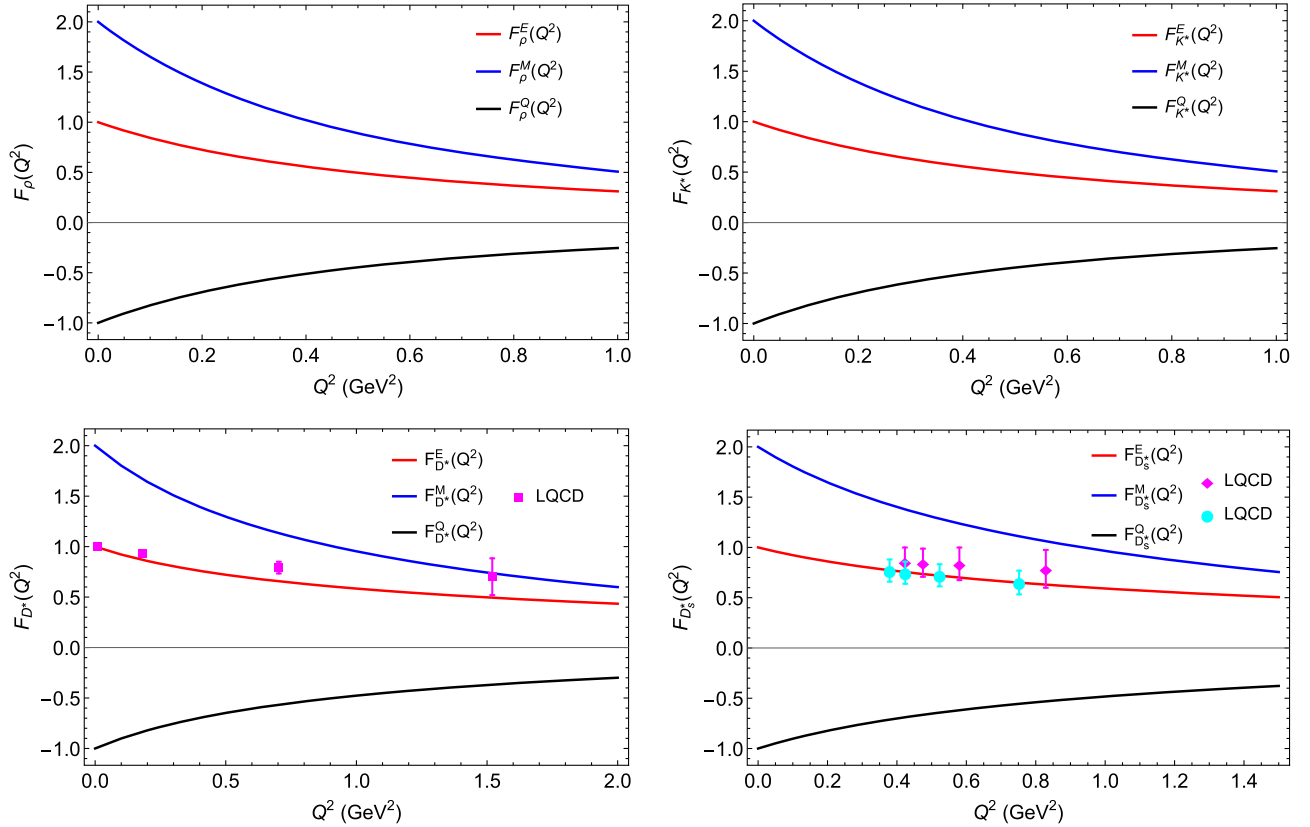

FIG. 1. The electric (red), magnetic (blue), and quadrupole (black) form factors of the vector mesons (ρ: top-left, K^*: top-right, D^*: bottom-left, D_s^*: bottom-right). The lattice QCD data for the electric form factor of D^*, and D_s^* are taken from Ref. [16] with $m_\pi = 300$ MeV and [17] for $m_\pi = 300$ MeV (cyan points) and $m_\pi = 315$ MeV (magenta points), respectively.
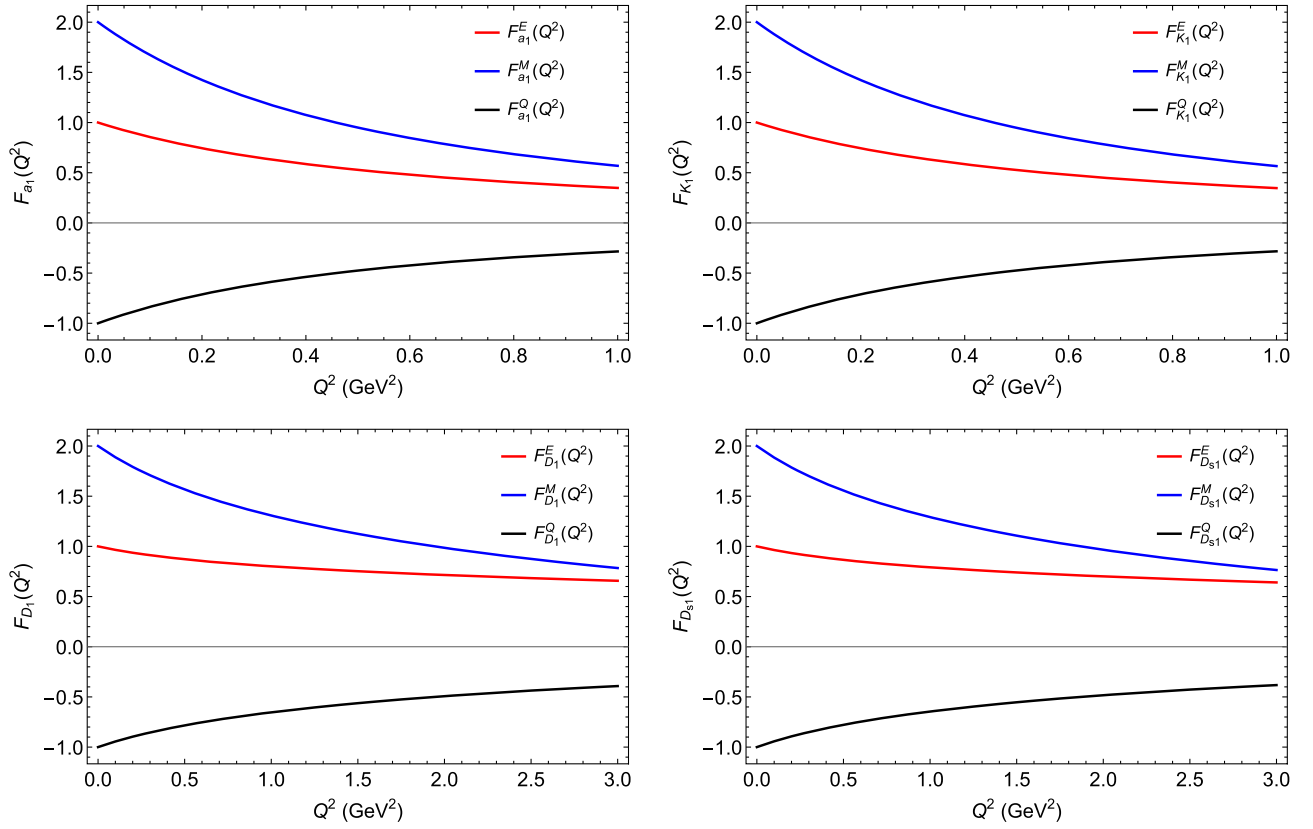
FIG. 2. The electric (red), magnetic (blue), and quadrupole (black) form factors of the axial vector mesons (a_1: top-left, K_1: top-right, D_1: bottom-left, D_{1s}: bottom-right).

$Q^2 = 0$ are well defined for the ground states of the four vector mesons studied in this work, ρ, K^*, D^*, and D_s^*, such that $F_{V^a}^E(0) = 1$, $F_{V^a}^M(0) = 2$, and $F_{V^a}^Q(0) = -1$. Unfortunately, the experimental data are not available for the EM form factors of the vector mesons. However, one can find the lattice QCD result for the D^* meson in the Ref. [16] with $m_\pi = 300$ MeV, and Ref. [17] provided two sets of solutions for the D_s^* based on a different value of the lattice spacing and pion mass ($m_\pi = 300$ MeV, and $m_\pi = 315$ MeV). From Fig. 1, one can see that the electric form factors of the D^* and D_s^* mesons are compatible with the lattice QCD results.

Similarly, we display the results of the electric, magnetic, and quadrupole form factors of the axial vector mesons in Fig. 2. Experimental data and lattice QCD results are currently unavailable for the axial vector sector. We hope that experimental and lattice QCD collaborations will report these results in the future. Our results for the axial vector mesons are comparable to those studied in the hard-wall holographic approach [39]. Finally, we examine the form factors of the π, K, D, and D_s mesons, and present the results in Fig. 3.

The pion form factor has been extensively studied from both theoretical and experimental perspectives. Previous works have investigated the pion form factor within the hard-wall and soft-wall holographic QCD models for the two-flavor case [36,42,44,50]. Experimental data for the pion form factor have been reported by the Jefferson Lab Collaboration for $Q^2 = 0.60$–2.45 GeV [2].

There are different lattice QCD results, and we compare our results with the ones reported by JLQCD [18], ETMC [19], and Lattice Hadron Physics (LHP) [20] Collaborations. Figure 3 demonstrates that our result is consistent with the lattice QCD result reported in Ref. [20], although discrepancies with experimental data have been reported in earlier works within holographic QCD [36,42,44,50]. Moreover, the comparison of the kaon form factor with the experimental data at low Q^2 [3] is shown in Fig. 3 (top-left). One can see that our prediction is in very good agreement with the available data. For the case of the D^0 and D_s mesons, only the data from the lattice QCD are available. The results of the EM form factors for D^0 and D_s mesons are shown in Fig. 3 (bottom-right) and (bottom-left), respectively. Our model's predictions are well consistent with the lattice QCD data.

From the results comparing with data, we can see that the form factors in the charm sector are in good agreement with experimental data, but for light mesons, especially for pion, the form factor deviates from the experimental data.
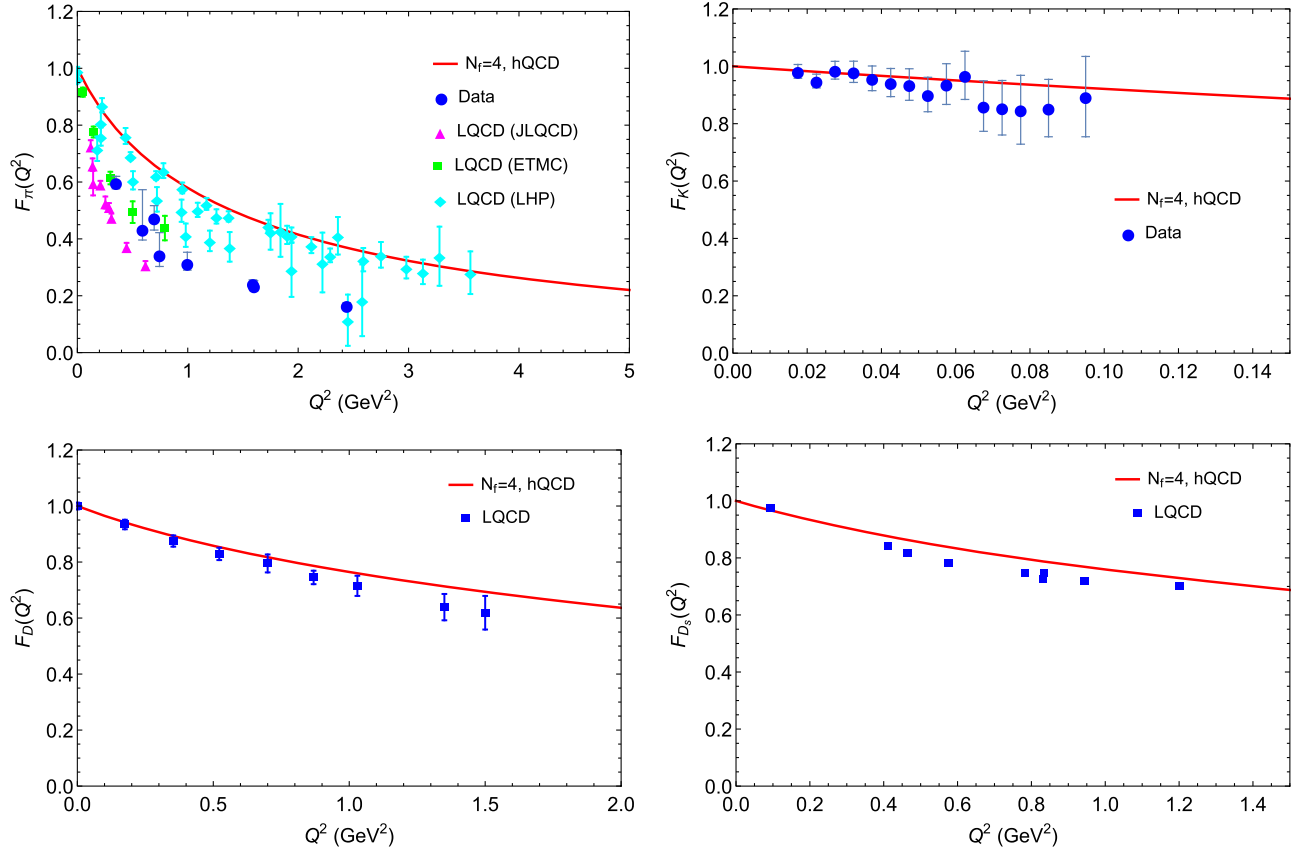
FIG. 3.   The form factors of the pseudoscalar mesons (π: top-left, K: top-right, D: bottom-left, D_s: bottom-right). The pion form factor is compared with the experimental data (blue points) [2] and LQCD data which are magenta points [18], green points [19], and cyan points [20]. The kaon form factor is compared with the experimental data in Ref. [3]. The lattice results from which the D and D_s mesons are compared to are taken from Refs. [16,21], respectively.

E. Charge radii

We calculate the charge radii of vector, axial vector, and pseudoscalar mesons in holographic QCD using Eq. (53). The results are presented in Table VII. We compare the charge radii of the pion and kaon with the values listed by the PDG [53]. For the D^+ and D^{*+} mesons, we compare our results with lattice data from Ref. [16]. Similarly, we compare the D_s^+ and D_s^{*+} mesons with lattice data from Refs. [21,17]. However, there are no available experimental or lattice results for the remaining mesons' charge radii. It is seen that the charge radii of the pion are in 65% agreement with the experimental data, and the D_s^{*+} meson is in 95% agreement with the experimental data.

TABLE VII.   Set of predictions for charge radius, compared to experimental or lattice QCD data.

Observable	$N_f = 4$, hQCD (fm)	Data (fm)
r_{π^+}	0.43	0.66 [53]
r_{K^+}	0.45	0.56 [53]
r_{D^+}	0.29	0.37 [16]
$r_{D_s^+}$	0.31	0.35 [21]
r_{ρ^+}	0.65	
$r_{K^{*+}}$	0.65	
$r_{D^{*+}}$	0.57	0.44 [16]
$r_{D_s^{*+}}$	0.46	0.44 [17]
$r_{a_1^+}$	0.62	
$r_{K_1^+}$	0.62	
$r_{D_1^+}$	0.28	
$r_{D_{s1}^+}$	0.32	

VI. CONCLUSIONS

In the present work, we performed the four flavors modified soft-wall holographic model to investigate various aspects of mesons, including meson spectra, decay constants, electromagnetic form factors, and charge radii of the vector, axial vector, and pseudoscalar mesons. The model parameters were fitted to experimental meson masses and decay constants, enabling us to obtain the meson spectra for the vector mesons, ρ, K^*, ω, D^*, D_s^*, and J/ψ, axial vector mesons, a_1, K_1, f_1, D_1, D_{s1}, and χ_{c1}, and pseudoscalar mesons, π, K, η, D, D_s, and η_c. By considering the higher-order terms in action in our model, comparing the meson

spectra with the results obtained in Ref. [41], our results are significantly improved, especially for the pseudoscalar sector. Moreover, the decay constants were also computed and reported in Table V. In the vector sector, we predicted the decay constants of the K^*, D^*, and D_s^* mesons and compared the result for the ρ meson with experimental data, revealing a discrepancy of 16%. In the axial vector sector, the decay constant of the a_1 meson exhibited excellent agreement with the experimental data. Additionally, the decay constants of the pion and kaon were well reproduced in our model and compared with the experimental data, while the comparison for D and D_s mesons were made with lattice data.

Considering the strong coupling constants of the $g_{\rho\pi\pi}$, $g_{\rho KK}$, $g_{\rho DD}$, $g_{\rho\rho\rho}$, $g_{\rho K^*K^*}$, $g_{\rho D^*D^*}$, $g_{\rho a_1 a_1}$, $g_{\rho K_1 K_1}$, and $g_{\rho D_1 D_1}$, we investigated the $SU(4)$ flavor symmetry breaking. The results demonstrated that flavor symmetry is broken due to the different values of the quark masses and condensates, as indicated in Table VI.

Furthermore, we studied the electromagnetic form factors and charge radii of the mesons of ρ, K^*, D^*, D_s^*, a_1, K_1, D_1, D_{s1}, π, K, D, and D_s. In the vector sector, our predicted electric form factors for D^* and D_s^* were found to be compatible with available lattice data. The predicted results of the axial vector mesons' electric, magnetic, and quadruple form factors are shown in Fig. 2. For the pion meson, our work has a discrepancy with the experimental data; however, it is in agreement with the lattice results from Ref. [20], as depicted in Fig. 3. Moreover, the kaon form factor exhibited good agreement with experimental data at low Q^2, similar to the results for D and D_s mesons, which also aligned well with lattice data. Finally, we calculated the charge radii using the holographic QCD. The obtained values are provided in Table VII, where we predicted and compared the results with the available experimental or lattice data.

From these results, we can see that the physical quantities in the charm sector are in good agreement with experimental data, but for light flavor mesons, the model predictions deviate away from the experimental data. This may indicate that the realization of chiral symmetry breaking in the light flavor sector needs to be improved further.

ACKNOWLEDGMENTS

[1] S. R. Amendolia *et al.* (NA7 Collaboration), Nucl. Phys. **B277**, 168 (1986).

[2] G. M. Huber *et al.* (Jefferson Lab Collaboration), Phys. Rev. C **78**, 045203 (2008).

[3] S. R. Amendolia, G. Batignani, G. A. Beck, E. H. Bellamy, E. Bertolucci, G. Bologna, L. Bosisio, C. Bradaschia, M. Budinich, M. Dell'orso *et al.*, Phys. Lett. B **178**, 435 (1986).

[4] T. M. Aliev and M. Savci, Phys. Rev. D **70**, 094007 (2004).

[5] V. V. Braguta and A. I. Onishchenko, Phys. At. Nucl. **68**, 1211 (2005).

[6] Y. Z. Xu, D. Binosi, Z. F. Cui, B. L. Li, C. D. Roberts, S. S. Xu, and H. S. Zong, Phys. Rev. D **100**, 114038 (2019).

[7] S. Cheng, Phys. Rev. D **100**, 013007 (2019).

[8] D. Jin and Y. D. Yang, Chin. Phys. C **36**, 941 (2012).

[9] U. Raha and A. Aste, Phys. Rev. D **79**, 034015 (2009).

[10] D. Stamen, D. Hariharan, M. Hoferichter, B. Kubis, and P. Stoffer, Eur. Phys. J. C **82**, 432 (2022).

[11] C. W. Hwang, Phys. Rev. D **81**, 054022 (2010).

[12] H. Y. Cheng, C. K. Chua, and C. W. Hwang, Phys. Rev. D **69**, 074025 (2004).

[13] R. C. Verma, J. Phys. G **39**, 025005 (2012).

[14] C. W. Hwang, Eur. Phys. J. C **23**, 585 (2002).

[15] J. Yu, B. W. Xiao, and B. Q. Ma, J. Phys. G **34**, 1845 (2007).

[16] K. U. Can, G. Erkol, M. Oka, A. Ozpineci, and T. T. Takahashi, Phys. Lett. B **719**, 103 (2013).

[17] S. S. Cui, N. Li, and Y. J. Wu, Int. J. Mod. Phys. A **34**, 1950194 (2019).

[18] T. Kaneko *et al.* (JLQCD and TWQCD Collaborations), Proc. Sci. LATTICE2008 (**2008**) 158 [arXiv:0810.2590].

[19] R. Frezzotti, V. Lubicz, and S. Simula (ETM Collaboration), Phys. Rev. D **79**, 074506 (2009).

[20] F. D. R. Bonnet *et al.* (Lattice Hadron Physics Collaboration), Phys. Rev. D **72**, 054506 (2005).

[21] N. Li and Y. J. Wu, Eur. Phys. J. A **53**, 56 (2017).

[22] J. Erlich, E. Katz, D. T. Son, and M. A. Stephanov, Phys. Rev. Lett. **95**, 261602 (2005).

[23] L. Da Rold and A. Pomarol, Nucl. Phys. **B721**, 79 (2005).

[24] A. Karch, E. Katz, D. T. Son, and M. A. Stephanov, Phys. Rev. D **74**, 015005 (2006).

[25] S. S. Gubser and A. Nellore, Phys. Rev. D **78**, 086007 (2008).

[26] S. S. Gubser, A. Nellore, S. S. Pufu, and F. D. Rocha, Phys. Rev. Lett. **101**, 131601 (2008).

[27] J. Grefa, J. Noronha, J. Noronha-Hostler, I. Portillo, C. Ratti, and R. Rougemont, Phys. Rev. D **104**, 034002 (2021).

[28] U. Gursoy and E. Kiritsis, J. High Energy Phys. 02 (2008) 032.

[29] U. Gursoy, E. Kiritsis, and F. Nitti, J. High Energy Phys. 02 (2008) 019.

[30] Y. Chen, D. Li, and M. Huang, Commun. Theor. Phys. **74,** 097201 (2022).

[31] D. Li, M. Huang, and Q. S. Yan, Eur. Phys. J. C **73,** 2615 (2013).

[32] D. Li and M. Huang, J. High Energy Phys. 11 (2013) 088.

[33] M. A. Martin Contreras, E. Folco Capossoli, D. Li, A. Vega, and H. Boschi-Filho, Nucl. Phys. **B977,** 115726 (2022).

[34] M. A. M. Contreras, E. F. Capossoli, D. Li, A. Vega, and H. Boschi-Filho, Phys. Lett. B **822,** 136638 (2021).

[35] X. Cao, M. Baggioli, H. Liu, and D. Li, J. High Energy Phys. 12 (2022) 113.

[36] R. Chen, D. Li, K. Bitaghsir Fadafan, and M. Huang, Chin. Phys. C **47,** 063106 (2023).

[37] Z. Abidin and C. E. Carlson, Phys. Rev. D **80,** 115010 (2009).

[38] D. Li and M. Huang, J. High Energy Phys. 02 (2017) 042.

[39] A. Ballon-Bayona, G. Krein, and C. Miller, Phys. Rev. D **96,** 014017 (2017).

[40] S. Momeni and M. Saghebfar, Eur. Phys. J. C **81,** 102 (2021); **82,** 709(E) (2022).

[41] Y. Chen and M. Huang, Phys. Rev. D **105,** 026021 (2022).

[42] H. R. Grigoryan and A. V. Radyushkin, Phys. Rev. D **76,** 115007 (2007).

[43] H. J. Kwee and R. F. Lebed, J. High Energy Phys. 01 (2008) 027.

[44] H. J. Kwee and R. F. Lebed, Phys. Rev. D **77,** 115007 (2008).

[45] H. Z. Sang and X. H. Wu, arXiv:1004.4392.

[46] Z. Abidin and P. T. P. Hutauruk, Phys. Rev. D **100,** 054026 (2019).

[47] H. R. Grigoryan and A. V. Radyushkin, Phys. Lett. B **650,** 421 (2007).

[48] H. R. Grigoryan and A. V. Radyushkin, Phys. Rev. D **76,** 095007 (2007).

[49] P. Colangelo, F. De Fazio, F. Giannuzzi, F. Jugeau, and S. Nicotri, Phys. Rev. D **78,** 055009 (2008).

[50] T. Gherghetta, J. I. Kapusta, and T. M. Kelley, Phys. Rev. D **79,** 076003 (2009).

[51] K. Chelabi, Z. Fang, M. Huang, D. Li, and Y. L. Wu, Phys. Rev. D **93,** 101901 (2016).

[52] C. A. Ballon Bayona, H. Boschi-Filho, N. R. F. Braga, and M. A. C. Torres, J. High Energy Phys. 01 (2010) 052.

[53] P. A. Zyla et al. (Particle Data Group), Prog. Theor. Exp. Phys. **2020,** 083C01 (2020).

[54] J. F. Donoghue, E. Golowich, and B. R. Holstein, Cambridge Monogr. Part. Phys., Nucl. Phys., Cosmol. **2,** 1 (1992).

[55] N. Isgur, C. Morningstar, and C. Reader, Phys. Rev. D **39,** 1357 (1989).

[56] M. E. Bracco, M. Chiapparini, F. S. Navarra, and M. Nielsen, Prog. Part. Nucl. Phys. **67,** 1019 (2012).